Additive Manufacturing 35 (2020) 101335

Contents lists available at ScienceDirect

Additive Manufacturing

journal homepage: www.elsevier.com/locate/addma

3D printing of clay for decorative architectural applications: Effect of solids volume fraction on rheology and printability

Shareen S.L. Chan[a], Ryan M. Pennings[b], Lewis Edwards[b], George V. Franks[a,*]

[a] Chemical Engineering, Melbourne School of Engineering, University of Melbourne, 3010, VIC, Australia
[b] MSD Robotics Lab, Architecture, Building and Planning, University of Melbourne, 3010, VIC, Australia

ARTICLE INFO

Keywords:
Ceramics
Material extrusion
Additive manufacturing (AM)
Direct ink writing (DIW)
Clay

ABSTRACT

The effect of varying the solids volume fraction of an aqueous clay paste suspension on its printability via an Additive Manufacturing (AM) or 3D printing technique, Direct Ink Writing (DIW) or material extrusion, has been studied. DIW is a cost-effective and straightforward fabrication technology suitable for adoption at a larger scale by the traditional ceramics industry and the creative community. The pastes were prepared with volume fraction of solids ranging from 25–57 vol%. Their rheological properties (storage modulus and apparent yield stress) were measured by dynamic oscillatory rheometry. The relationships between solids content, rheological behaviour and print parameters were evaluated. An equation based on rheological properties to delineate between printable and non-printable conditions has been proposed. Several decorative pieces have been produced for architectural purposes.

1. Introduction

Additive Manufacturing (AM), also known as Solid Freeform Fabrication (SFF), Rapid Prototyping (RP) or 3D printing, is a group of techniques which fabricate structures on a layer-by-layer basis directly from 3D data. It is often referred to as one of the disruptive technologies revolutionizing product development and manufacturing [1]. The edge AM has over traditional manufacturing techniques lies in the reduction in processes and resources required to produce geometrically complex, near-net-shape structures. In certain designs, the shapes cannot be produced by conventional processing technologies.

Although there has been significant research on AM of polymeric and metallic materials in the last three decades, work on ceramic materials is still rather limited [2]. There are challenges in processing ceramic materials by AM, such as in terms of feedstock and sintering [3]. Also, because of their brittle nature, ceramics are inherently different from polymers and metals in that defects in the 3D printing process will dramatically reduce the strength and reliability of the component. Although advances have been made to eliminate defects, it is an ongoing challenge. As such 3D printed ceramics generally are not currently qualified for structural applications that require high reliability such as in human occupied air vehicles. On the other hand, decorative features in architectural applications do not require high strength. 3D printing enables a wider range of possible shapes for the artist to produce.

Several AM technologies have been put forward for the fabrication of complex ceramic architectures, such as Selective Laser Melting/Sintering (SLM/SLS) [4], binder jetting [5], robocasting or Direct Ink Writing (DIW) [2], Fused Deposition Modelling of Ceramics (FDM/FDC) [6], ink-jetting [7], stereolithography (SLA) [8], and Digital Light Processing (DLP) [9].

Powder bed processes (i.e. SLM/SLS, binder jetting) tend to result in porous structures due to the nature of the powder bed. Therefore, vat polymerization (i.e. SLA, DLP) and slurry-based deposition (i.e. DIW, FDM/FDC, ink-jetting) are typically the preferred techniques for dense ceramic parts. However, slurry-based AM technologies create green bodies that still require post-printing binder burnout and sintering to densify the ceramic structures.

Among the slurry-based methods, the DIW technique is considered one of the most reliable and widely-used techniques [2,3,10]. By extruding a filament of highly viscous paste through a nozzle (generally at room temperature), the nozzle traverses across the platform in the designed shape layer by layer to build up the 3D part. It is relatively inexpensive and faster than photocuring AM techniques, and it possesses the ability to fabricate freestanding structures with little need for supports [11]. Nonetheless, it is not without limitations. For example, it has been reported that drying in air during DIW limits the minimum diameter of the nozzle to approximately 0.5 mm, below which clogging

* Corresponding author.
E-mail address: gvfranks@unimelb.edu.au (G.V. Franks).

https://doi.org/10.1016/j.addma.2020.101335
Received 17 December 2019; Received in revised form 28 April 2020; Accepted 13 May 2020
Available online 20 May 2020

occurs [3].

The majority of the scientific publications on DIW of ceramic materials seems to be advanced ceramics, such as zirconia, barium titanate and boron carbide [2]. Despite traditional ceramics such as clay, being a large industry sector, there are relatively few papers on this new advanced technology [12,13]. On the other hand, 3D printing of cement-based mortars has garnered relatively more interest in both industrial applications [14–16] and literature [17–19], probably due to their ubiquitous use in contemporary architecture. Clay is also used as a minor additive to cements and geopolymers to aid in printability [19,20]. Occasionally, DIW of clay-based materials is used in construction projects [21,22]. An increased use of clay-based mortars is greatly beneficial to the environment [23]. More recently, advances have been made in DIW of clays [12,24,25], including substantial focus on tool path planning particularly when robotic arms are used to deliver the clay [26,27].

It is recognized that well-controlled viscoelastic response is essential for flow through the print nozzle and promptly retaining the filament shape after deposition [28]. Therefore, it is important to understand the rheological properties of the paste and how they relate to the success of the DIW print. Smay et al. [29] proposed a minimum value of storage modulus for printing spanning geometries, calculated as

$$G^{'} \geq 1.4\rho g\left(\frac{L}{D}\right)^{4} D \tag{1}$$

where G' is the storage modulus of the paste, ρ is the density of the paste, L is the distance between the centre of two adjacent filaments (i.e. span), and D is the filament diameter. Recent work by Barki and coworkers [30] accounted for the effects of gravity and capillary forces, and after re-arrangement of equations, their criterion for a minimum yield stress can be written as:

$$\tau_y \geq \gamma D^{-1} + \rho g h \tag{2}$$

where τ_y is the shear yield stress, γ is the suspension's surface tension, D is the nozzle diameter, g is gravitational acceleration, and h is the height of the printed part.

The main objective of this research is to explore the relationships between the volume fraction of solids of the clay paste inks, their rheological properties, and the suitable printing parameters. A preformulated throwing clay has been procured and mixed with water (e.g. manually or pugging) before forming, so that only the amount of water is varied in the experiment, without the introduction of additives. With a better understanding of their process-properties-performance relationships, it would be beneficial to the traditional ceramics industry and even individual artists in adopting DIW for clay. In particular, decorative features could be added in architectural design either in the restoration of older buildings (e.g. replacing damaged gargoyles), or new artistic features in modern designs.

2. Materials and methods

2.1. Clay

A commercially available throwing clay (AA103 PB103 Fine White Stoneware, Walker Ceramics, Australia), comprised of mainly clays, quartz and feldspar, was purchased. To determine the phase composition X-ray diffraction (XRD) was performed on an oven-dried sample of the clay that was ground with a mortar and pestle. Diffraction data was collected using a Bruker D8 Advance X-ray diffractometer with Ni-filtered Cu kα radiation (1.54 Å). Data was collected between $5-85^{\circ}$ 2θ, with a step size of 0.02° and a scan rate of 1.0 s per step. An anti-scatter blade was used to reduce the diffracted background intensity at low angles. An incident beam divergence of 1.0° was used with a 2.5° soller slit in the diffracted beam. The sample was spun at 15 revolutions per minute. Phase identification was completed using Diffrac.EVA V4.1 software with the ICDD PDF4 + 2018 database. Quantitative phase analysis was conducted with open-source software MAUD (Materials Analysis Using Diffraction) [31].

The particle size distribution of the clay was measured using a laser diffraction particle size analyser (Mastersizer 3000, Malvern, UK). The clay was dispersed into Reverse Osmosis water so that measurements were conducted at laser obscuration levels of 10%, 14% and 18%, with 3 measurements taken at each level. A refractive index of 1.56 and absorption index of 0.01 were utilized. The moisture content of the as-received commercially-procured clay was determined by drying samples in the oven at 80 °C for more than 48 h. The difference in masses before and after drying was the amount of water in the original clay mixture.

2.2. Preparation of paste suspensions

Additional reverse osmosis (RO) water was added to the clay in varying amounts to obtain samples of different solids volume fraction. For printing with the Bioplotter, pastes with 25, 30, 34, 38, 42, 50 vol% solids were formulated. The clay with the added RO water was mixed manually with a spatula due to the small volume. The pastes were loaded into 30 mL plastic disposable syringe barrels, followed by a piston at the larger opening of the barrel.

Larger batches for the robots were mixed in a pug mill (VPM7-SS, Peter Pugger, Ukiah CA, USA). Water was added to clay in the pug mill, which after mixing was pugged (extruded out the end). Pugged clay was stored in a container, while the process was repeated until a suitable amount of clay was made. Once mixed the printing cartridges were attached to the end of the pug mill, and clay was pugged into them. This resulted in the elimination of most air bubbles during filling. Pastes with solid fractions of 50, 52, 53, 55 and 57 vol% were formulated for use with the robots.

2.3. Rheology measurements

Rheological properties of the suspensions were characterised using a controlled shear rate and shear stress rheometer (MCR702 TwinDrive Rheometer, Anton Paar, Germany). The steady state viscosity as a function of shear rate was measured from 0.01–10 s^{-1}, using a four-bladed vane of 10 mm diameter and 20 mm length, and cylindrical cup of 30 mm inner diameter, at 22 °C. The storage modulus was measured in the same vane-in-cup geometry. Oscillatory measurements were conducted at a constant angular frequency of 10 rad/s, and an increasing shear strain from 0.01 to 200%. The measured torque values were converted to stress using the geometry [32]. The storage modulus (G') and the loss modulus (G'') were determined from the phase difference between the applied strain and measured stress [33]. In this work, when we refer to the storage modulus, we mean the value of the plateau in the storage modulus at shear stresses approaching zero. The shear stress at the intersection of the storage modulus and the loss modulus is referred to as the apparent yield stress in this paper.

2.4. DIW of suspensions

Printability of the suspensions was determined by extrusion of the pastes through nozzles of various diameters. Two instruments were used. First, a commercially available pressure-controlled DIW system (3D-Bioplotter, EnvisionTEC, Germany) was used for smaller diameter nozzles. Nozzle inner diameters ranged from 0.26 to 1.27 mm. The pneumatic pressure was from 0.1–5.0 bar, which is the feasible range of the equipment. Print speeds used ranged from 6 to 25 mm/s. The inner fill was a log-pile lattice structure that was produced by layers of parallel printed lines, with alternating layers of perpendicular lines. (see Fig. 1A)

The second instrument was an adhesive dispensing system (Techcon, Cypress CA, USA) repurposed for clay extrusion. This configuration of this system is common within the clay 3D printing field.

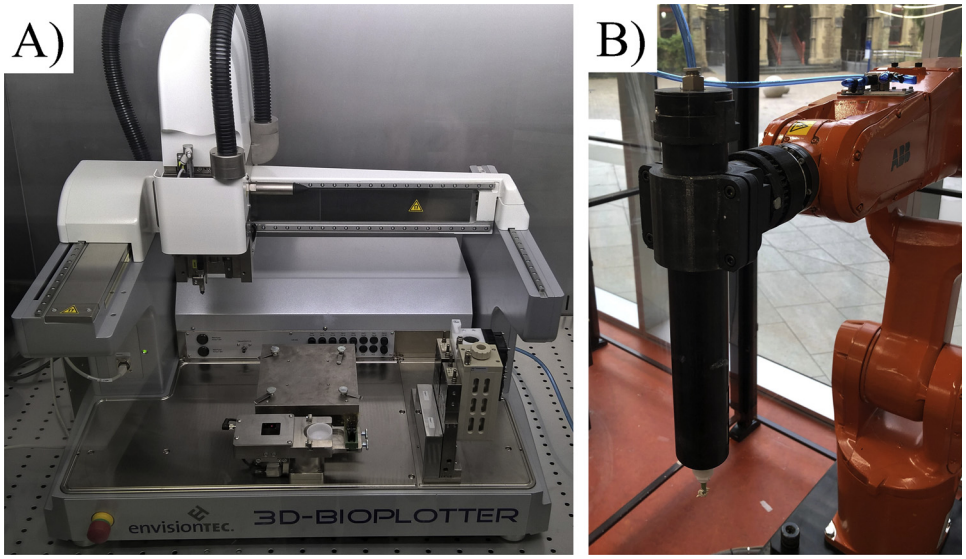

Fig. 1. Photographs of A) EnvisionTEC 3D-Bioplotter used for printing with smaller nozzle sizes, and B) robotic arm and extruder used for printing with larger nozzle sizes.

The system was attached to a 6-axis robotic arm (IRB 120, ABB, Switzerland). Nozzle diameters between 0.51 mm and 3 mm were used. Typical pneumatic pressures ranged from 1.4–6.9 bar, and speeds ranged from 1 to 80 mm/s though 80 mm/s was most commonly used (see Fig. 1B).

2.5. Sintering

After the printing process, the green bodies were exposed to air of ambient conditions to dry for a minimum of 24 h. Next the dried samples were sintered in air at atmospheric pressure in a furnace (F25 Furnace, Tetlow, Australia). The sintering was conducted at 1250 °C for 1 h, with a dwell at 400 °C for 30 min to burn out any organics. A temperature ramp of 5 °C/min was applied during heating, and 10 °C/min during cooling.

2.6. Density measurements

For the printed decorative features, their bulk densities and porosities were measured using the Archimedes' method. RO water was used as the liquid medium for density measurement. The relative density was calculated by the following equations:

$$\rho_B = \frac{Dry\ Wt.}{Saturated\ Wt. - Submerged\ Wt.};$$
$$Relative\ density = \frac{\rho_B}{\rho_{TD}} \times 100\% \quad (3)$$

where ρ_B is bulk density and ρ_{TD} is theoretical density assumed to be 2600 kg/m^3.

3. Results

3.1. Characterization of clay

The XRD analysis indicates that clay consists of 44.0 wt% silica (quartz), 35.4 wt% kaolinite, and 18.8 wt% feldspar (microcline) with 1.8 wt% other minor components (see Fig. S 1 and Table S 1 for details). The particle size analysis (see Fig. S 2 and Table S 2 for details) revealed a maximum particle diameter (d_{100}) of 128 µm, and a median diameter (d_{50}) of 8.41 µm. Two peaks were observed at approximately 0.6 µm and 5 µm. The solids content of the as-received clay was found to be 57 vol% solids. The morphology of the particles was not investigated but it is expected that the silica and feldspar particles are equiaxed and the kaolinite particles are in the form of plate-like layers, which is known to contribute to the plastic behaviour of clay [34].

3.2. Effect of solids fraction on rheology

Fig. 2 shows the typical viscosity as a function of shear rate for paste suspensions with solids content from 25–57 vol%. For all the pastes, the viscosity decreases with increasing shear rate, which is typical of shear thinning ceramic particle suspensions. This property makes them suitable as an ink for DIW, as the ink would not drip from the nozzle before printing, starts flowing when sufficient stress is applied, and finally reverts to a solid-like mass that retains its shape shortly after deposition [28]. Fig. 3A shows the storage modulus as a function of shear stress for the paste suspensions from 25 to 50 vol% solids, which were printed with the Bioplotter. Fig. 3B is a similar plot for the paste suspensions from 50 to 57 vol% solids, which were printed using the robotic arm with larger nozzle sizes. A low shear stress plateau in *G'* is observed for all the pastes typical of linear viscoelastic fluids. In this region, *G"* was found to be an order of magnitude lower than *G'* as shown in Fig. S 3 in the supplementary materials section. Both Fig. 3A and 3B contain results for 50 vol% solids pastes measured on two different days. There is a slight difference in the two samples due to slightly different methods of preparation. Direct comparison of these two results is shown in Fig. S

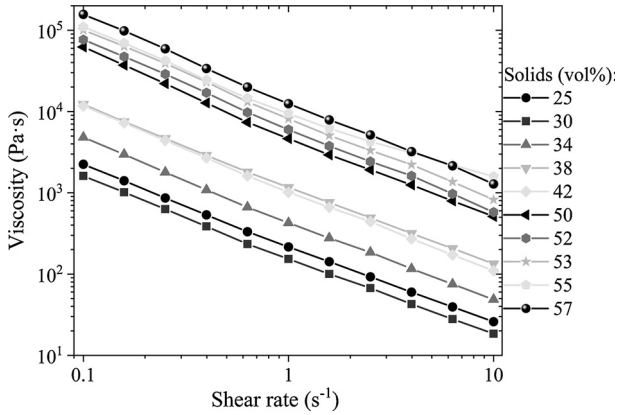

Fig. 2. Viscosity against shear rate for aqueous clay paste suspensions of 25 to 57 vol% solids.

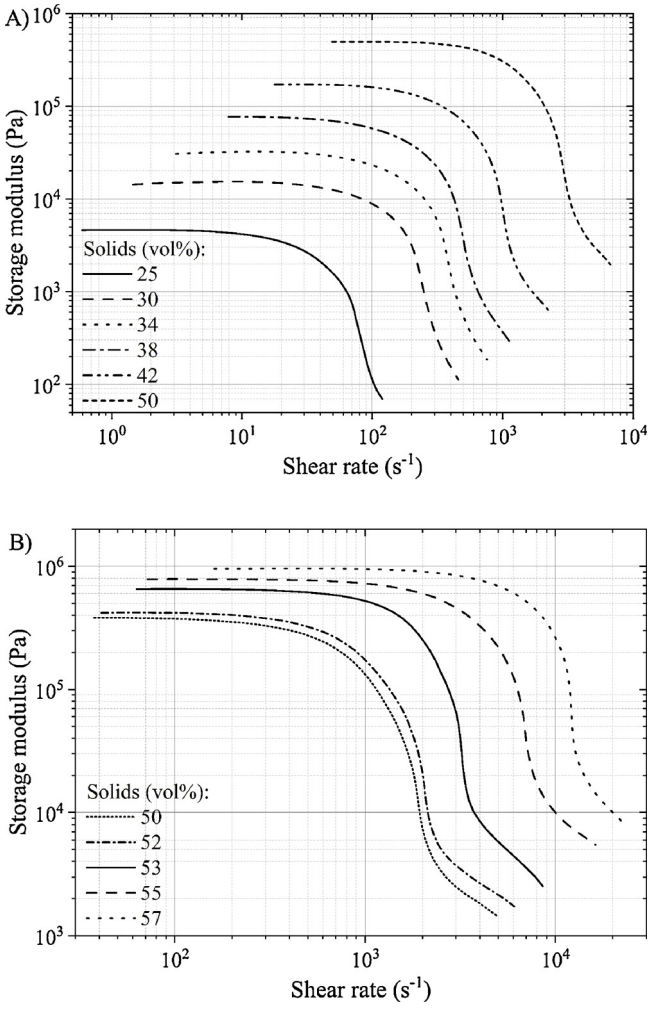

Fig. 3. Storage modulus against shear rate for clay pastes of solids content A) from 25 to 50 vol%, printed using the Bioplotter, and B) from 50 to 57 vol%, printed using the robotic arm. Plateau at region of low shear stress, typical of linear viscoelastic fluids.

4 in the supplementary materials section.

With a decreasing amount of water (and increasing volume fraction of solids), the suspension demonstrated an increasing storage modulus and yield stress as shown in Fig. 4. The storage modulus and yield stress were found to be power law functions of the volume fraction of solids, which is consistent with other literature [35–37] on particulate fluids:

$$G' = A\Phi^{a} \tag{4}$$

$$\tau_y = B\Phi^{b} \tag{5}$$

where G' is the storage modulus, τ_y is the yield stress, Φ is the volume fraction, and A, B, a, b are empirical constants. These parameters have been found to be $A = 9.77 \times 10^{-6}$, $B = 5.38 \times 10^{-8}$, $a = 6.26$ and $b = 6.44$, consistent with values in literature for attractive particle suspensions [35–37].

3.3. Effect of rheology on printability through various nozzle diameters

Slumping of the printed strands can occur to such an extent that the object cannot maintain its shape (see Fig. 5). Clogging happens when the paste is unable to be extruded out of the nozzle regardless of pressure applied up to about 5 bar and within a reasonable time frame. Fig. 6 shows the printability diagram relating storage modulus and nozzle diameter to slumping, clogging and printable regions. The value of the storage modulus increases with increasing volume fraction as

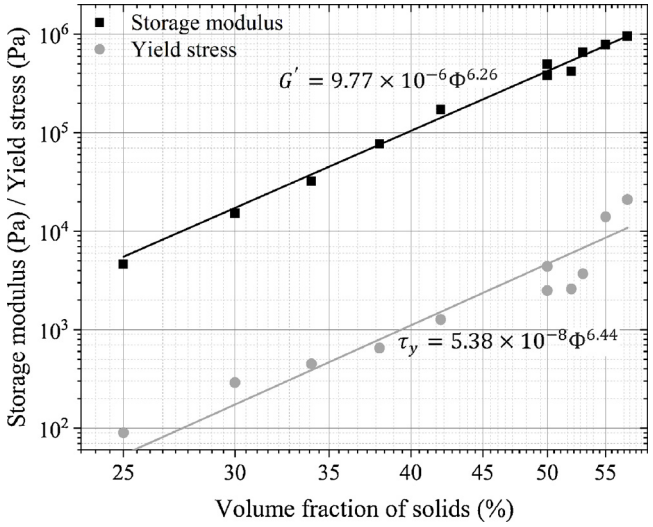

Fig. 4. Storage modulus and yield stress are observed to have a power law dependency on the volume fraction of solids.

explained in Section 3.2. At nozzle diameters of 0.26 mm or 0.30 mm and below, clogging is deemed to have occurred, preventing the ink from extruding even when the maximum pressure (5 bar) of the equipment is applied. Below a threshold value of storage modulus (for nozzles greater than about 0.3 mm), slumping always occurs (Fig. 6). Above this threshold value, components can be printed and hold their shape. The threshold value of modulus is about 20,000 Pa. Also, above a threshold modulus of about 700,000 Pa, printing becomes increasingly difficult, requiring a very high pressure or very low speed, or apparently clogging at smaller nozzle sizes. A similar map of printability is observed for yield stress and nozzle diameter (see Fig. S 5 in Supplementary Materials). In this case, the threshold value for yield stress is approximately 350 Pa, above which printed parts exhibit shape retention. In terms of solids loading, pastes in the range of 34–55 vol% were found to extrude well and also maintain its shape after deposition. This range corresponds with literature – Zocca and colleagues [3] noted a typical ceramic solid loading of 35–55 vol%, while recent work on clay with additives demonstrated positive results with 50 vol% solids [25].

3.4. Relationships between print pressure, speed and nozzle size

Fig. 7 shows the ratio of print pressure to print speed (= pressure/speed) as a function of nozzle size for clay pastes with volume fractions between 25 and 57 vol% solids. Fig. 7A presents the results for the pastes printed with the Bioplotter and Fig. 7B are the results for the pastes printed in the robot. The print speeds for the Bioplotter range from 6 to 25 mm/s and the pressures range from 0.1 to 5 bar. For the robot, the print speeds range from 1 to 80 mm/s and the pressures from 1.4 to 6.9 bar. Both sets of data indicate a decreasing print pressure to speed ratio with increasing nozzle size, although the trend is stronger for the data obtained from the robot. The data at similar nozzle size do not correspond most likely due to the different extruder designs resulting in different internal friction in the flow paths.

3.5. Effect of rheology on print parameters

The trend of increasing pressure-speed ratio with increasing storage modulus is shown in Fig. 8. If the print speed and nozzle size were maintained while the storage modulus is increased, a larger pressure would be required for printing. Furthermore, it can be generally observed that a smaller nozzle diameter would require a larger pressure-speed ratio. Similarly, Fig. S 6 illustrates an increase in the pressure-speed ratio when inks with higher yield stress are utilized. Also, when

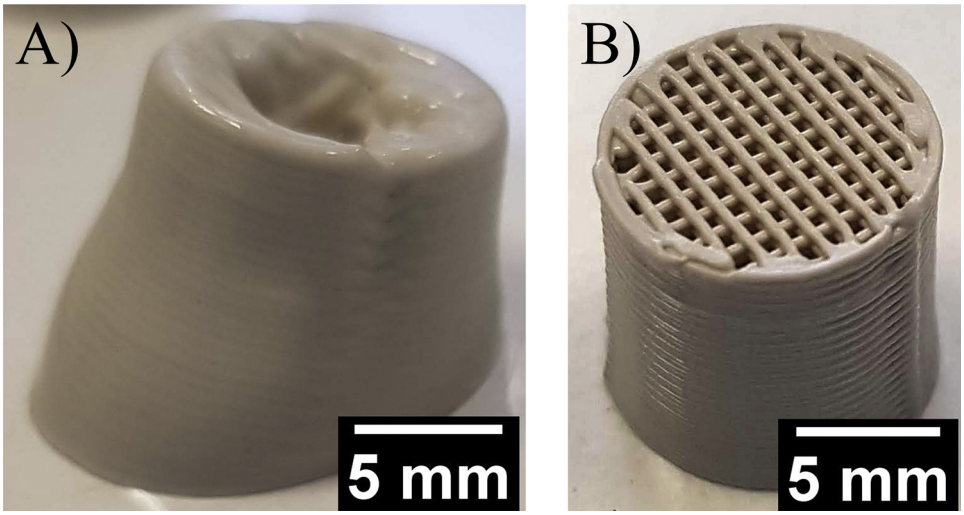

Fig. 5. Samples demonstrating: A) slumping after printing (25 vol% solids), and B) good printability without slumping (38 vol% solids).

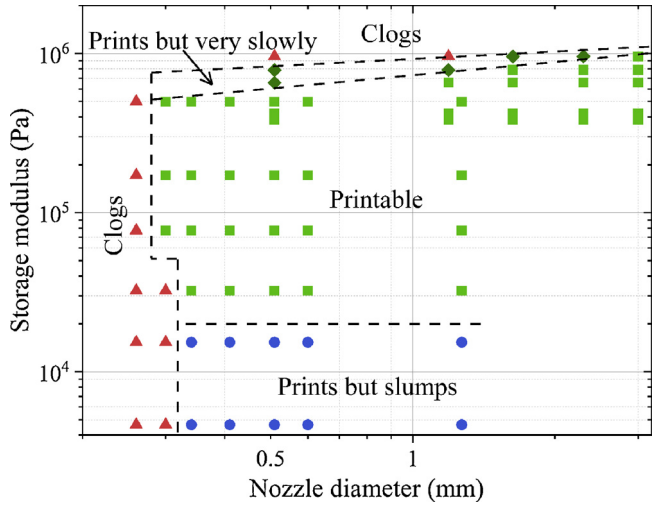

Fig. 6. Printability diagram of storage modulus against nozzle diameter. Clogging occurs below a critical nozzle diameter and above a threshold storage modulus. Slumping observed below a certain modulus.

smaller nozzle diameters are used, a higher pressure-speed ratio is required.

3.6. Complex shaped printed and sintered objects

Fig. 9 shows two relatively large printed objects with shapes that may be useful as decorative features in architectural design. The gargoyle demonstrates that features of historic buildings could be replaced using digital data (if such is available) to restore a building damaged by fire or other catastrophe such as the Cathedral of Notre Dame. The brick with wave features demonstrates that more modern designs can be rendered in clay by 3D printing. The bulk density of the sintered samples is 2370 kg/m^3 (91.2% of theoretical density) on average for the two different printed geometries shown in Fig. 9.

4. Discussion

4.1. Influence of solids fraction on rheology

By varying the solids volume fraction, the rheological properties of the clay suspension were changed. The yield stress of a suspension is related to the strength of the interparticle attraction and the number of

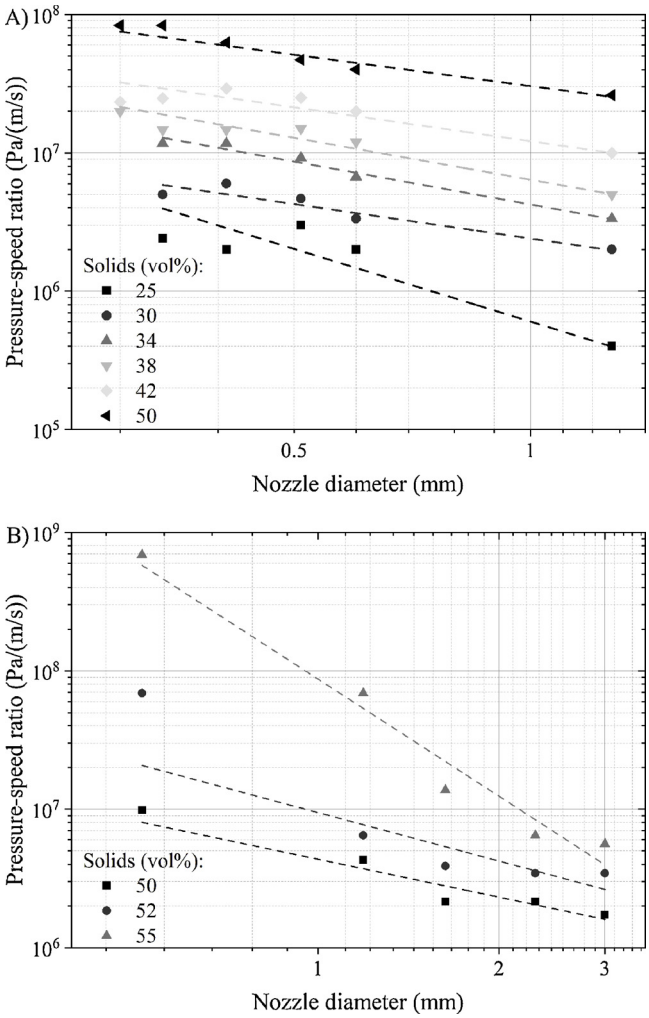

Fig. 7. Relationship between pressure-speed ratio and nozzle diameter, printed with A) the Bioplotter, and B) the robotic arm.

interparticle bonds to be broken [35]. In this work, since the same solid components (clay, quartz, feldspar and water) were used throughout, particle characteristics (i.e. network microstructure, size distribution, shape of particles) may be deemed as constant. Only solids volume fraction was changed in this investigation. With an increase in the solids

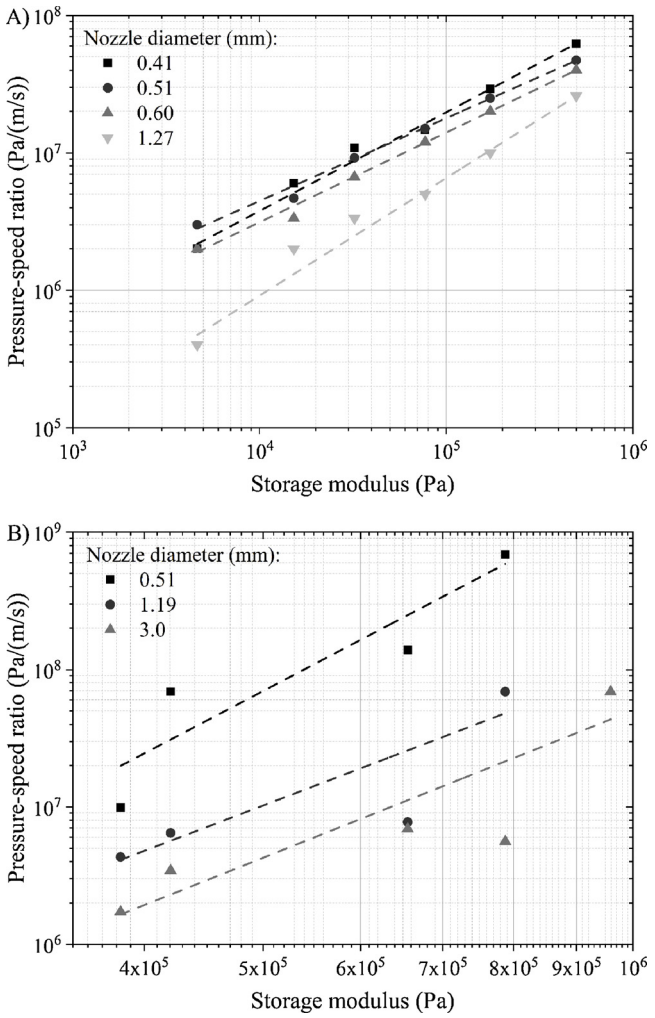

Fig. 8. Graph of print pressure-speed ratio versus storage modulus, for prints done on A) the Bioplotter, and B) the robotic arm. Inks with a higher storage modulus require a higher print pressure-speed ratio for printing. Smaller nozzle sizes also require a larger print pressure-speed ratio.

volume fraction, there are more particles per unit volume, which in turn means more particle-particle bonds per unit volume. Assuming the interparticle interaction forces do not change too much with water content, a higher stress is thus required to deform and break the increased number of bonds, leading to higher storage moduli and yield stresses, as was observed in Fig. 4. [38]

The theoretical shear modulus, G_0^{th}, for attractive interacting spherical colloidal particles can be estimated as

$$G_0^{th} = \frac{\tau}{\gamma} = \left(\frac{3}{32}\right)\frac{\phi_m n}{R}\left(\frac{\partial^2 V_T}{\partial d^2}\right) \tag{6}$$

where τ is the shear stress, γ is the shear strain, ϕ_m is the maximum volume fraction of packing, n is the average number of nearest neighbours, R is the average centre to centre distance of two neighbouring particles in the lattice and V_T is the total interaction energy between the particles [39]. With an increase in solids volume fraction, the solid particles are packed more densely and the number of contacting neighbours increases. This leads to a reduction in average interparticle distance, R, and increase in n, which in turn causes an increase in the shear modulus. The storage modulus, G', is a component of the shear modulus, particularly the in-phase response measured when an oscillatory shear force is applied. It is a measure of the energy stored elastically. Therefore, with an increase in solids volume fraction, there is an expected increase in the storage modulus, as demonstrated in Fig. 4.

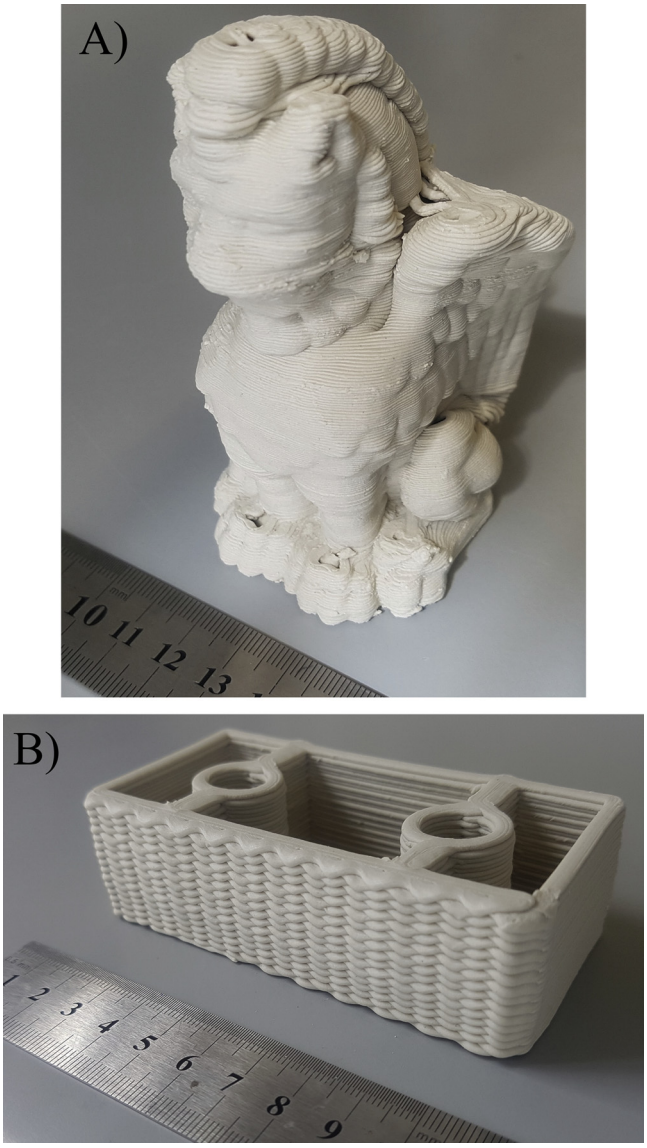

Fig. 9. Photographs of 3D-printed decorative features: A) gargoyle, a common feature in medieval architecture; and B) modern brick featuring waves on exterior side. There objects were printed from the 53 vol% solids paste through 2.3 mm diameter nozzles using the robot. The scales in the photos are in cm.

4.2. Print pressure, speed and nozzle size

An increase in yield stress with increasing solids fraction is a result of the increased bond density, as explained in Section 4.1. Therefore, a higher stress in terms of a higher print pressure is naturally required to break down the increased number of bonds, and to induce flow.

The Darcy-Weisbach equation for pipe flow is expressed as

$$\Delta P = f\frac{L}{D}\frac{\rho V^2}{2} \tag{7}$$

where ΔP is the pressure drop, f is the Darcy friction factor, L is the length of the pipe, D is the diameter of the pipe, ρ is the density of the fluid and V is the flow velocity. Assuming the print speed is maintained, the flow velocity, V, of the paste through and out of the nozzle remains the same. All other parameters are constant too, except for D which increases with an increase in nozzle diameter. The pressure drop, ΔP, across the nozzle is reduced, so a lower input pressure is required for the same flow velocity and print speed. Thereby reducing the pressure-speed ratio required for larger nozzles as shown experimentally in

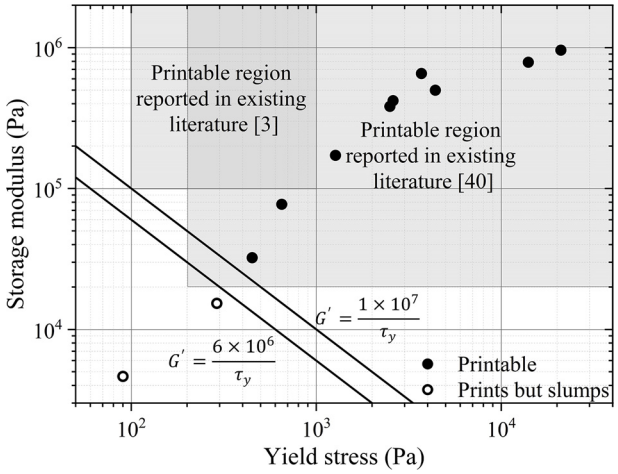

Fig. 10. Graph of storage modulus against yield stress, showing two regions of printability and proposed equation separating them.

Fig. 7.

We have demonstrated that it is possible to print by DIW using nozzles down to a diameter of 0.30 mm, which is a lower minimum than previously reported of 0.5 mm [3]. Our minimum nozzle diameter of 300 μm is about twice the maximum diameter of the particles of 128 μm. We postulate that the reason for clogging at lower nozzle sizes is due to two (or more) large particles locking up against each other, transverse to the cross-section of the nozzle, and blocking the flow, rather than drying in air. This is independent of rheological properties, so if finer features are required to be printed, the water-solids ratio appears to be less important. Instead, the original clay procured should contain particles of a maximum diameter smaller than one half the nozzle diameter.

4.3. Printability criterion

When the experimental data for printability verses slumping is compared to the predictions based on storage modulus by Smay et al. [29] in Eq. (1) (see Fig. S 7A), their predictions had difficulty in correctly predicting the pastes that slumped (indicated by the open circles). While compared to the predictions based on yield stress by Barki et al. [30] given by Eq. (2) (see Fig. S 7B), their predictions are quite accurate in predicting whether the pastes would slump or not. This motivates us to search for an improved printability criterion, especially related to the storage modulus.

Slumping was observed to occur for suspensions with lower values of both storage moduli and yield stresses (see Fig. 10). Existing literature reports that ceramic paste inks for DIW that are printable have storage moduli of 10^5–10^6 Pa and yield stress in the range 10^2– 10^3 Pa [3]. This is indicated as the rectangular region at the upper left of Fig. 10. Another team [40], reports that the modulus must be more than 2000 kPa and the yield stress must be more than 200 Pa [2,40]. This is indicated by the large rectangular region to the upper right of Fig. 10. We propose that instead of a fixed lower limit for G' and τ_y separately, there is a product relationship between G' and τ_y which forms the boundary transitioning from good printability to slumping. We propose the equation as

$$G' = \frac{K}{\tau_y} \tag{8}$$

where K is a constant. In this work, K is approximately within the range of 6×10^6 to 1×10^7. This new printability criterion is consistent with the previously published criteria [2,3,40].

Future work could include using clays with a different maximum particle size, to confirm whether the minimum nozzle diameter is dependent on that. Also, more data in terms of storage modulus-yield stress and their printability is required to establish the validity of the storage modulus-yield stress printability boundary equation proposed.

5. Conclusions

In this investigation, the water-to-solids content of a traditional clay mix was varied to effect changes in its rheological properties, which are in turn studied for their relationship to printability as a paste ink for Direct Ink Writing (DIW). The formulations with solids content between about 34 and 55 vol% solids produced pastes that attained a high level of printability without the use of additives.

The ability to print through different size nozzles was found not to be dependent on the rheological properties. Regardless of rheology, printing was unsuccessful for nozzle diameters less than about 0.26 to 0.30 mm. The limiting factor for this seems to be the particle size of the solids. Above the minimum nozzle size, printing is possible using larger nozzles in conjunction with a suitable combination of printing pressures and speeds.

The pressure-speed ratio required for printing was observed to increase with an increase in rheological properties, namely storage modulus and yield stress. Also, the pressure-speed ratio has shown an increasing trend with a decreasing nozzle size.

Pastes with too low a storage modulus and yield stress slump and the body cannot maintain its shape against gravity. Conversely, pastes with too high a storage modulus and yield stress cannot be extruded out of the nozzle and clog.

Lastly, we propose an equation to delineate printability from slumping that is related to the product of storage modulus and yield stress. It is a potential boundary separating the inks with rheological properties suitable for printing, from those which slump after being printed.

CRediT authorship contribution statement

Shareen S.L. Chan: Conceptualization, Methodology, Investigation, Writing - original draft. **Ryan M. Pennings:** Conceptualization, Investigation, Methodology, Software, Writing - review & editing. **Lewis Edwards:** Methodology, Software, Investigation. **George V. Franks:** Conceptualization, Writing - review & editing, Supervision, Project administration.

Declaration of Competing Interest

The authors declare that they have no known competing financial interests or personal relationships that could have appeared to influence the work reported in this paper.

Acknowledgments

This research is supported by an Australian Government Research Training Program (RTP) Scholarship. The authors would also like to thank Liz Goodall (Materials Characterisation and Fabrication Platform, University of Melbourne) and Will Ng for their work on the XRD analysis. Thanks to Mitchell Sesso and Daniel Riley for their technical and project planning discussions.

References

[1] I. Gibson, D. Rosen, B. Stucker, Additive Manufacturing Technologies: 3D Printing, Rapid, 2nd ed, Springer, 2015, https://doi.org/10.2497/jjspm.61.216.
[2] E. Peng, D. Zhang, J. Ding, Ceramic robocasting: recent achievements, potential, and future developments, Adv. Mater. 30 (2018) 1–14, https://doi.org/10.1002/adma.201802404.
[3] A. Zocca, P. Colombo, C.M. Gomes, J. Günster, Additive manufacturing of ceramics: issues, potentialities, and opportunities, J. Am. Ceram. Soc. 98 (2015) 1983–2001, https://doi.org/10.1111/jace.13700.

[4] S.L. Sing, W.Y. Yeong, F.E. Wiria, B.Y. Tay, Z. Zhao, L. Zhao, Z. Tian, S. Yang, Direct selective laser sintering and melting of ceramics: a review, Rapid Prototyp. J. 23 (2017) 611–623, https://doi.org/10.1108/RPJ-11-2015-0178.

[5] J. Moon, J.E. Grau, V. Knezevic, M.J. Cima, E.M. Sachs, Ink-jet printing of binders for ceramic components, J. Am. Ceram. Soc. 85 (2010) 755–762, https://doi.org/10.1111/j.1151-2916.2002.tb00168.x.

[6] A. Bellini, L. Shor, S.I. Guceri, New developments in fused deposition modeling of ceramics, Rapid Prototyp. J. 11 (2005) 214–220, https://doi.org/10.1108/13552540510612901.

[7] R. Noguera, M. Lejeune, T. Chartier, 3D fine scale ceramic components formed by ink-jet prototyping process, J. Eur. Ceram. Soc. 25 (2005) 2055–2059, https://doi.org/10.1016/j.jeurceramsoc.2005.03.223.

[8] M.L. Griffith, J.W. Halloran, Freeform fabrication of ceramics via stereolithography, J. Am. Ceram. Soc. 79 (2005) 2601–2608, https://doi.org/10.1111/j.1151-2916.1996.tb09022.x.

[9] G. Mitteramskogler, R. Gmeiner, R. Felzmann, S. Gruber, C. Hofstetter, J. Stampfl, J. Ebert, W. Wachter, J. Laubersheimer, Light curing strategies for lithography-based additive manufacturing of customized ceramics, Addit. Manuf. 1–4 (2014) 110–118, https://doi.org/10.1016/j.addma.2014.08.003.

[10] G.V. Franks, C. Tallon, A.R. Studart, M.L. Sesso, S. Leo, Colloidal processing: enabling complex shaped ceramics with unique multiscale structures, J. Am. Ceram. Soc. 100 (2017) 458–490, https://doi.org/10.1111/jace.14705.

[11] Z. Chen, Z. Li, J. Li, C. Liu, C. Lao, Y. Fu, C. Liu, Y. Li, P. Wang, Y. He, 3D printing of ceramics: a review, J. Eur. Ceram. Soc. 39 (2019) 661–687, https://doi.org/10.1016/j.jeurceramsoc.2018.11.013.

[12] C.F. Revelo, H.A. Colorado, 3D printing of kaolinite clay ceramics using the Direct Ink writing (DIW) technique, Ceram. Int. 44 (2018) 5673–5682, https://doi.org/10.1016/j.ceramint.2017.12.219.

[13] O. Kontovourkis, G. Tryfonos, C. Georgiou, Robotic additive manufacturing (RAM) with clay using topology optimization principles for toolpath planning: the example of a building element, Archit. Sci. Rev. 63 (2020) 105–118, https://doi.org/10.1080/00038628.2019.1620170.

[14] A. Cor, Apis Cor – Dubai Municipality: Largest 3D Printed Building to Date, (2019) https://www.apis-cor.com/dubai-project.

[15] Arup, Printed Buildings: Is This Construction's Digital Future? (2018) https://www.arup.com/projects/3d-housing-05.

[16] ICON, ICON + New Story + ECHALE Unveil First Homes in 3D-Printed Community, (2019) https://www.iconbuild.com/updates/first-3d-printed-home-community.

[17] M. Moini, J. Olek, J.P. Youngblood, B. Magee, P.D. Zavattieri, Additive manufacturing and performance of architectured cement-based materials, Adv. Mater. 30 (2018) 1–11, https://doi.org/10.1002/adma.201802123.

[18] N. Washburn, S. Ketel, G. Sant, B. Wang, G. Falzone, A printability index for linking slurry rheology to the geometrical attributes of 3D-printed components, Cem. Concr. Compos. 101 (2019) 32–43, https://doi.org/10.1016/j.cemconcomp.2018.03.022.

[19] S.M. Sajadi, P.J. Boul, C. Thaemlitz, A.K. Meiyazhagan, A.B. Puthirath, C.S. Tiwary, M.M. Rahman, P.M. Ajayan, Direct ink writing of cement structures modified with nanoscale additive, Adv. Eng. Mater. 21 (2019) 1801380, , https://doi.org/10.1002/adem.201801380.

[20] B. Panda, M.J. Tan, Experimental study on mix proportion and fresh properties of fly ash based geopolymer for 3D concrete printing, Ceram. Int. 44 (2018) 10258–10265, https://doi.org/10.1016/j.ceramint.2018.03.031.

[21] C. Scott, IAAC Demonstrates On Site Robotics 3D Printing Construction Method in Barcelona, (2017) https://3dprint.com/182052/iaac-3d-print-on-site-construction/.

[22] A. Chiusoli, The First 3D Printed House With Earth | Gaia (n.d.), (2020) https://www.3dwasp.com/en/3d-printed-house-gaia/.

[23] A.A. Shubbar, M. Sadique, P. Kot, W. Atherton, Future of clay-based construction materials – a review, Constr. Build. Mater. 210 (2019) 172–187, https://doi.org/10.1016/j.conbuildmat.2019.03.206.

[24] C.F. Revelo, H.A. Colorado, 3D printing of kaolinite clay with small additions of lime, fly ash and talc ceramic powders, Process. Appl. Ceram. 13 (2019) 287–299, https://doi.org/10.2298/PAC1903287R.

[25] E. Ordoñeza, J.M. Gallego, H.A. Colorado, 3D printing via the direct ink writing technique of ceramic pastes from typical formulations used in traditional ceramics industry, Appl. Clay Sci. 182 (2019) 105285, , https://doi.org/10.1016/J.CLAY.2019.105285.

[26] O. Kontovourkis, G. Tryfonos, Robotic 3D clay printing of prefabricated non-conventional wall components based on a parametric-integrated design, Autom. Constr. 110 (2020) 103005, , https://doi.org/10.1016/j.autcon.2019.103005.

[27] J. Hergel, K. Hinz, S. Lefebvre, B. Thomaszewski, Extrusion-based ceramics printing with strictly-continuous deposition, ACM Trans. Graph. 38 (2019) 1–11, https://doi.org/10.1145/3355089.3356509.

[28] J.A. Lewis, Direct ink writing of 3D functional materials, Adv. Funct. Mater. 16 (2006) 2193–2204, https://doi.org/10.1002/adfm.200600434.

[29] J.E. Smay, J. Cesarano, J.A. Lewis, Colloidal inks for directed assembly of 3-D periodic structures, Langmuir. 18 (2002) 5429–5437, https://doi.org/10.1021/la0257135.

[30] A. M'Barki, L. Bocquet, A. Stevenson, Linking rheology and printability for dense and strong ceramics by direct ink writing, Sci. Rep. 7 (2017) 1–10, https://doi.org/10.1038/s41598-017-06115-0.

[31] L. Lutterotti, Total pattern fitting for the combined size-strain-stress-texture determination in thin film diffraction, Nucl. Instruments Methods Phys. Res. Sect. B Beam Interact. Mater. Atoms. 268 (2010) 334–340, https://doi.org/10.1016/j.nimb.2009.09.053.

[32] N.Q. Dzuy, D.V. Boger, Direct yield stress measurement with the vane method, J. Rheol. (N. Y. N. Y). 29 (1985) 335–347, https://doi.org/10.1122/1.549794.

[33] H.A. Barnes, J.F. Hutton, K. Walters, An Introduction to Rheology, Elsevier Science, 1989.

[34] H. Van Olphen, An introduction to clay colloid chemistry, for clay technologists, geologists, and soil scientists., an Introd. To Clay Colloid Chem, Clay Technol. Geol. Soil Sci. (1977).

[35] G.V. Franks, S.B. Johnson, P.J. Scales, D.V. Boger, T.W. Healy, Ion-specific strength of attractive particle networks, Langmuir. 15 (1999) 4411–4420, https://doi.org/10.1021/la9815345.

[36] R. de Rooij, D. van den Ende, M.H.G. Duits, J. Mellema, Elasticity of weakly aggregating polystyrene latex dispersions, Phys. Rev. E 49 (1994) 3038–3049, https://doi.org/10.1103/PhysRevE.49.3038.

[37] A.A. Potanin, R. De Rooij, D. Van den Ende, J. Mellema, Microrheological modeling of weakly aggregated dispersions, J. Chem. Phys. 102 (1995) 5845–5853, https://doi.org/10.1063/1.469317.

[38] Z. Zhou, M.J. Solomon, P.J. Scales, D.V. Boger, The yield stress of concentrated flocculated suspensions of size distributed particles, J. Rheol. (N. Y. N. Y). 43 (1999) 651–671, https://doi.org/10.1122/1.4890747.

[39] R. Eriksson, H. Pajari, J.B. Rosenholm, Shear modulus of colloidal suspensions: comparing experiments with theory, J. Colloid Interface Sci. 332 (2009) 104–112, https://doi.org/10.1016/j.jcis.2008.12.034.

[40] C. Minas, D. Carnelli, E. Tervoort, A.R. Studart, 3D printing of emulsions and foams into hierarchical porous ceramics, Adv. Mater. 28 (2016) 9993–9999, https://doi.org/10.1002/adma.201603390.